DRAFT VERSION JUNE 8, 2020
Typeset using LaTeX **twocolumn** style in AASTeX62

Cluster Difference Imaging Photometric Survey (CDIPS) II: A Jupiter-Sized Planet Candidate in IC 2602

L. G. BOUMA,[1] R. BRAHM,[2,3,4] J. D. HARTMAN,[1] P. EVANS,[5] G. ZHOU,[6] J. DE LEON,[7] C. BERGMANN,[8] K. G. STASSUN,[9,10] K. A. COLLINS,[6] S. N. QUINN,[6] C. .G. TINNEY,[8,11] C. ZIEGLER,[12] C. BRICEÑO,[13] N. LAW,[14] A. W. MANN,[14] J. LIVINGSTON,[7] T. HENNING,[15] A. JORDÁN,[16,4] N. ESPINOZA,[17] W. BHATTI,[1] J. N. WINN,[1] G. Á. BAKOS,[1] G. R. RICKER,[18] R. VANDERSPEK,[18] D. W. LATHAM,[6] S. SEAGER,[19] J. M. JENKINS,[20] AND TSO/SPOC/POC REPRESENTATIVES

[1]*Department of Astrophysical Sciences, Princeton University, 4 Ivy Lane, Princeton, NJ 08540, USA*
[2]*Center of Astro-Engineering UC, Pontificia Universidad Católica de Chile, Av. Vicuña Mackenna 4860, 782-0436 Macul, Santiago, Chile*
[3]*Instituto de Astrofísica, Facultad de Física, Pontificia Universidad Católica de Chile, Av. Vicuña Mackenna 4860, 782-0436 Macul, Santiago, Chile*
[4]*Millennium Institute of Astrophysics, Av. Vicuña Mackenna 4860, 782-0436 Macul, Santiago, Chile*
[5]*El Sauce Observatory, Coquimbo Province, Chile*
[6]*Center for Astrophysics | Harvard & Smithsonian, 60 Garden St, Cambridge, MA 02138, USA*
[7]*Department of Astronomy, University of Tokyo, 7-3-1 Hongo, Bunkyo-ky, Tokyo 113-0033, Japan*
[8]*Exoplanetary Science at UNSW, School of Physics, UNSW Sydney, NSW 2052, Australia*
[9]*Vanderbilt University, Department of Physics & Astronomy, 6301 Stevenson Center Lane, Nashville, TN 37235, USA*
[10]*Fisk University, Department of Physics, 1000 17th Avenue N., Nashville, TN 37208, USA*
[11]*Australian Centre for Astrobiology, UNSW Sydney, NSW 2052, Australia*
[12]*Dunlap Institute for Astronomy and Astrophysics, University of Toronto, 50 St. George Street, Toronto, Ontario M5S 3H4, Canada*
[13]*Cerro Tololo Inter-American Observatory, Casilla 603, La Serena, Chile*
[14]*Department of Physics and Astronomy, The University of North Carolina at Chapel Hill, Chapel Hill, NC 27599-3255, USA*
[15]*Max-Planck-Institut für Astronomie, Königstuhl 17, 69117 Heidelberg, Germany*
[16]*Facultad de Ingeniería y Ciencias, Universidad Adolfo Ibáñez, Av. Diagonal las Torres 2640, Peñalolén, Santiago, Chile*
[17]*Space Telescope Science Institute, 3700 San Martin Drive, Baltimore, MD 21218, USA*
[18]*Department of Physics and Kavli Institute for Astrophysics and Space Research, Massachusetts Institute of Technology, Cambridge, MA 02139, USA*
[19]*Department of Earth, Atmospheric, and Planetary Sciences, Massachusetts Institute of Technology, Cambridge, MA 02139, USA*
[20]*NASA Ames Research Center, Moffett Field, CA 94035, USA*

(Received June 8, 2020; Revised —; Accepted —)

Submitted to AAS journals.

ABSTRACT

We validate the planetary nature of the transiting planet TOI 837.01. We characterize the system using data from the NASA *Transiting Exoplanet Survey Satellite* (TESS), the ESA Gaia mission, ground-based photometry, and spectroscopy from CTIO1.5/CHIRON, MPG2.2/FEROS, and AAT/Veloce. We find that TOI 837 is a $T = 9.9$ G-dwarf in IC 2602 (the "Southern Pleiades"). The star is therefore 30 ± 20 million years old. The validated planet is warm ($P = 8.YY$ d) and likely Jupiter-sized. However, its transits are grazing: $b > 0.92$ at 3σ. From transit photometry alone, the planetary size lies within 0.58–3.87 $R_{\rm Jup}$, due to the degeneracy between the planetary size and its impact parameter. From radial velocity monitoring, we find that its mass is less than 2.XX $M_{\rm Jup}$ (3σ). This mass limit requires the planetary size to be below $\approx 2.0 R_{\rm Jup}$. Non-planetary explanations for the data, most notably hierarchical or background eclipsing binaries, are argued to be highly unlikely on statistical grounds. TOI 837.01 therefore tentatively joins the ranks of adolescent exoplanets orbiting bright host stars. Further analysis of its mass, atmosphere, and obliquity could confirm its planetary nature beyond doubt, and are worthwhile because young planets do interesting things.

Keywords: Exoplanets (XXX), Exoplanet evolution (491), Stellar ages (1581), Young star clusters (XXX)

1. INTRODUCTION

Recently, young planets have been hype.
TESS (Ricker et al. 2015).
Section 2 Section 3 Section 5 Section 6 Section 7.

Corresponding author: L. G. Bouma
luke@astro.princeton.edu

2. THE DATA

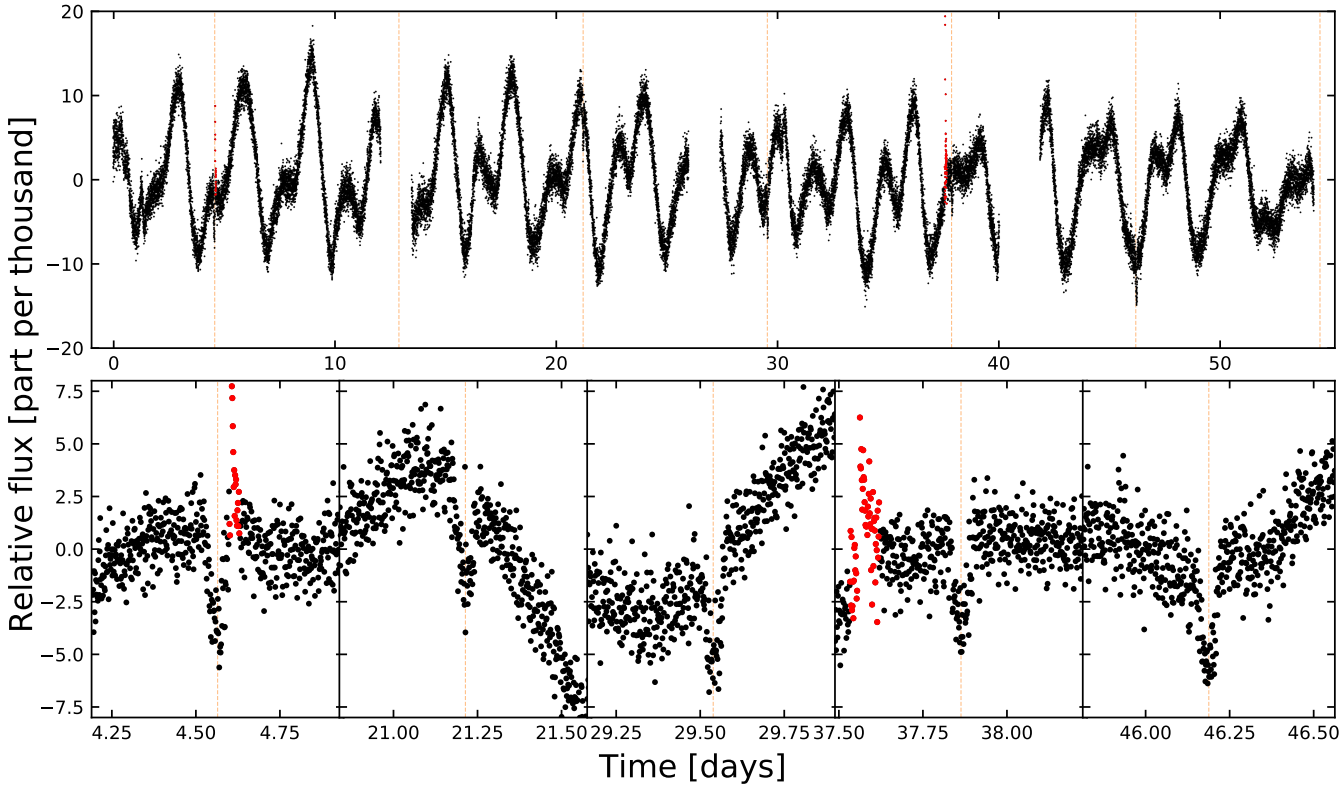

Figure 1. TESS lightcurve of TOI 837 (Sectors 10 and 11). *Top*: PDCSAP mean-subtracted relative flux at 2-minute sampling. Spot-induced stellar variability is the dominant signal. Dashed lines show the five transits observed by TESS. *Bottom*: Zoomed windows of individual transits. Red points show manually identified stellar flares.

2.1. *TESS Photometry*

TOI 837 (GAIA DR2 5251470948229949568) was observed by the TESS spacecraft from X to Y in two-minute cadence mode. The star was designated TIC 460205581 in the TESS Input Catalog (Stassun et al. 2018, 2019). The pixel data for an 11×11 array surrounding TOI 837 were averaged into 2-minute stacks by the onboard computer. Each 2048×2048 image from the CCD was also averaged into 30-minute stacks, and saved as a "full frame image" (FFI).

The pixel data for an The 2-minute stacks for TOI 837 were reduced to lightcurves by the Science Processing Operations Center (SPOC) at NASA Ames (Jenkins et al. 2016). We mainly used the Presearch Data Conditioning (PDC) lightcurve. The PDC lightcurve aperture used pixels chosen to maximize the SNR of the total flux of the target (**?**). Non-astrophysical variability was removed by fitting out trends common to many stars (**??**).

As an independent check on the 2-minute SPOC lightcurve, we examined the lightcurve based upon 30-minute image stacks which was produced as part of the Cluster Difference Imaging Photometric Survey (CDIPS; Bouma et al. 2019). Our CDIPS lightcurve of choice used a circular aperture with radius 1 pixel.

Figure 1.

2.2. *Ground-based Time-Series Photometry*

2.3. *Imaging*

2.4. *Spectroscopy*

2.4.1. *CHIRON*

9 spectra with CTIO1.5/CHIRON, from January 28 through March 14, 2020. 6 were usable.

2.4.2. *FEROS*

N spectra with XXX/FEROS

2.4.3. *Veloce*

M spectra with AAT/Veloce.

2.5. *Astrometry*

3. THE STAR

3.1. *The Cluster*

IC 2602 canonically has an age of 30 ± 20 Myr (CITE: Van Leeuwen 2009). Or logage between 7.533 and 7.563 (Bossini et al. 2019).

Or Li age of 40-50Myr (David+19, comparison with other Li stars).

Reported mean metallicity values [Fe/H] for the cluster range between slightly super-solar (0.04 ± 0.01, Baratella et al. 2020) and slightly sub-solar (-0.02 ± 0.02, Netopil et al. 2016).

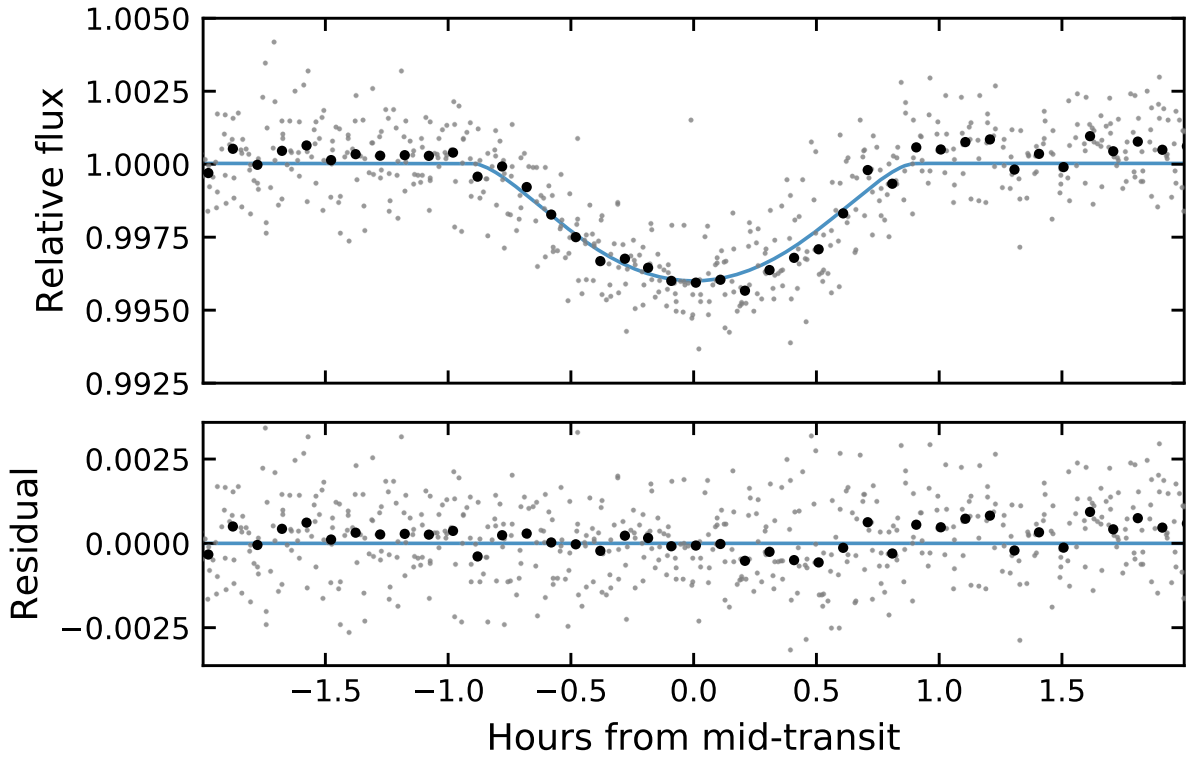

Figure 2. Phase-folded transit of TOI 837.01. Gray points are 2-minute PDCSAP flux measurements, detrended with a 0.3-day robust Huber spline (see Section 2.1). Black points are binned to approximately 1 point per 6 minutes. The blue line shows the transit model corresponding to the median transit parameters (Table 2).

IC 2602 is supervirial, in the sense that the observed stellar velocity dispersion is larger than the value expected if it were in virial equilibrium by about a factor of two (Bravi et al. 2018).

"""Although IC 2602 does not belong to Sco OB2, it is spatially and dynamically a close relative, and for this reason we include it in this work, if even marginally"" (Damiani+2019). """We also find that the open cluster IC 2602 has a similar dynamics to Sco OB2, and its PMS members are currently evaporating and forming a diffuse (size 10deg) halo around its double-peaked core"""

3.2. *Cluster Membership*

TOI 837 has been reported as a member of IC 2602 by multiple independent investigators (Kharchenko et al. 2013; Cantat-Gaudin et al. 2018).

The Gaia kinematics are good; gamma velocity is correct; Li (FEROS + Veloce) is strong; the rotation period and vsini agree with sub-Pleiades age expected for an IC 2602 member.

3.2.1. *HR Diagram*

Figure 3 shows a Hertzsprung-Russell diagram of TOI 837 in reference to the broader IC 2602 cluster, as well as its neighborhood. Cluster members were identified by Cantat-Gaudin et al. (2018) using using Gaia-DR2 positions, proper motions, and parallaxes. We included candidate members with formal membership probability exceeding 10%. Save for a few low-mass outliers, most members appear to be young and coeval.

TOI 837 is in its expected position relative to the other members along the cluster isochrone. This photometrically limits the presence of binary companions in the TOI 837 system, to a magnitude difference of perhaps half the brightness of the target star.

Figure 3 also suggests that the membership census of IC 2602 is incomplete. We defined the reference "neighborhood" as the group of at most 10^4 randomly selected non-member stars within 5 standard deviations of the mean IC 2602 right ascension, declination, and parallax. We queried Gaia DR2 for these stars using `astroquery` (Ginsburg et al. 2018). Many low-mass stars appear above the main sequence, even though they were not identified as 5-dimensional kinematic members through the unsupervised **?** membership assignment process.

3.2.2. *Position and Kinematics*

We examine the six-dimensional positions and kinematics in greater depth in Figure 4. The "neighborhood" is defined here identically to as in Figure 3. The axes limits for the right ascension, declination, and parallax dimensions are as in the Gaia archive query. The axes limits for the proper motion and radial velocity dimensions are set at the 25th and 75th percentiles, in order to give a sense of the population's distribution, while excluding outlying points. The radial velocities

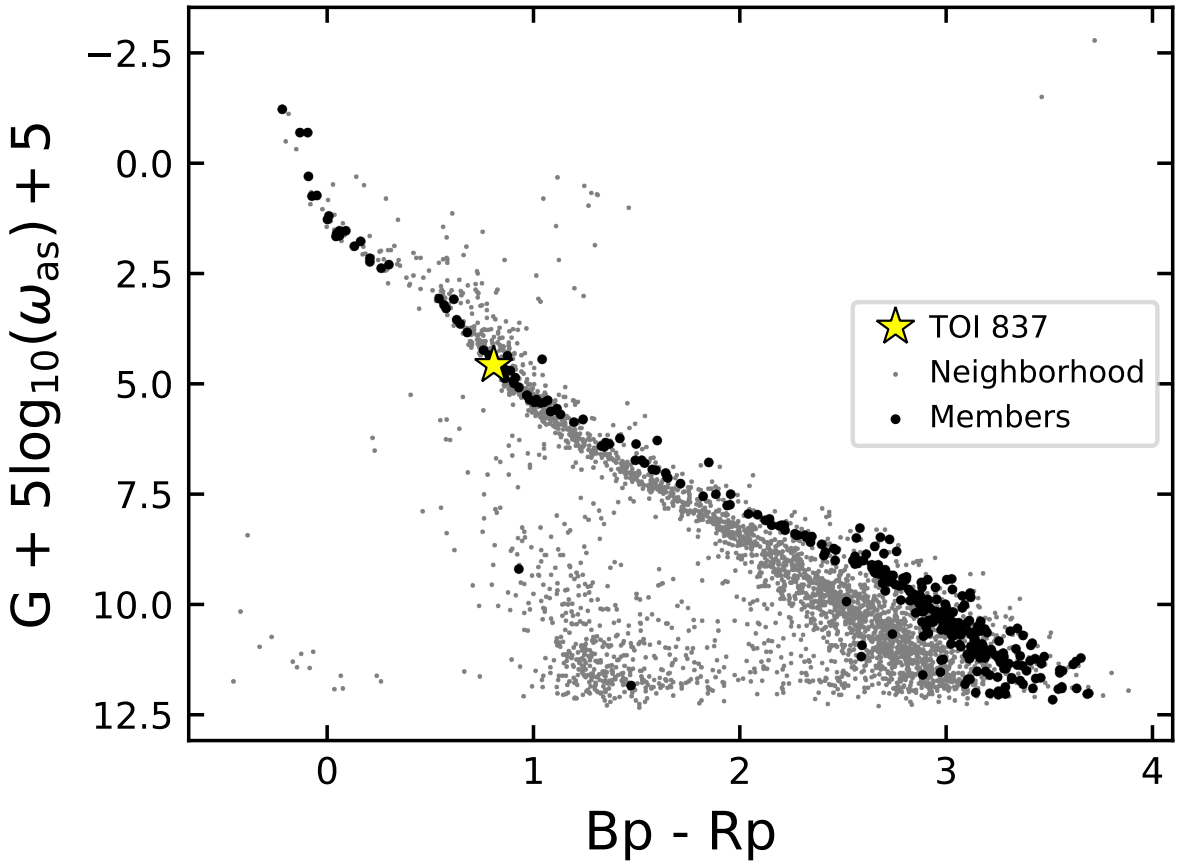

Figure 3. Hertzsprung-Russell diagram of TOI 837 and members of IC 2602. Members (black circles) were identified by Cantat-Gaudin et al. (2018). Gray circles are non-member stars within 5 standard deviations of the mean IC 2602 right ascension, declination, and parallax. *G* denotes Gaia broadband magnitudes, *Bp* Gaia blue, *Rp* Gaia red, and ω_{as} the parallax in arcseconds.

suffer the greatest incompleteness due to the current $G \approx 12$ magnitude limit of the Gaia-DR2 data processing.

Figure 4 provides strong evidence *(i)* for the existence of the IC 2602 open cluster and *(ii)* for the membership of TOI 837 within IC 2602. The only dimension that could perhaps lead to some worry is the parallax, as TOI 837 is one of the closest IC 2602 members reported by Cantat-Gaudin et al. (2018). Fortunately, there are independent means of verifying stellar youth.

3.2.3. *Rotation*

TESS photometric rotation period = 3.5days ish. vsini = 17.48 ± 0.15 (CHIRON). The two agree.

For comparison, gyrochrones would "predict" X.XX.

This implies sub-Pleiades age expected for an IC 2602 member.

Figure 5 compares the stellar rotation period of TOI 837 to periods that have been measured in a number of well-studied open clusters. TOI 837 seems to be gyrochronologically coeval with the Pleiades sequence.

We note that this is still in the "sub 500 Myr" range, when classical Skumanich spin-down is not expected to be happening (why is this the number?).

This agrees with recent empirical results from Rebull et al 2020 and perhaps also 2018(?): they observed the Taurus foreground (age 30 Myr) and saw that it was roughly consistent with the Pleaides. Upper Sco had a consistent mean, but a much larger scatter.

3.2.4. *Lithium*

Rafael's co-added FEROS spectra gave a Li doublet equivalent width of 154 milliangstrom.

Lithium depletion for a star of TOI-837's spectral type happens over timescales >100 Myr (Soderblom+2013). This is because the convective envelopes are very shallow, so they don't cycle material down to the >3e6 K core until much later.

Nonetheless, comparison of early-G field stars to e.g., 600 Myr old Hyads has shown that the depletion does happen over gigayear timescales (Berger+2018, fig 7).

Figure 6 compares our measured TOI 837 Li EW to stars in the field, and to young open cluster members. The field star measurements were collected by Berger et al. (2018). We have shown the points with lithium detections at SNR > 3. TOI-837 is consistent with being younger than almost all CKS planet-hosting field stars.

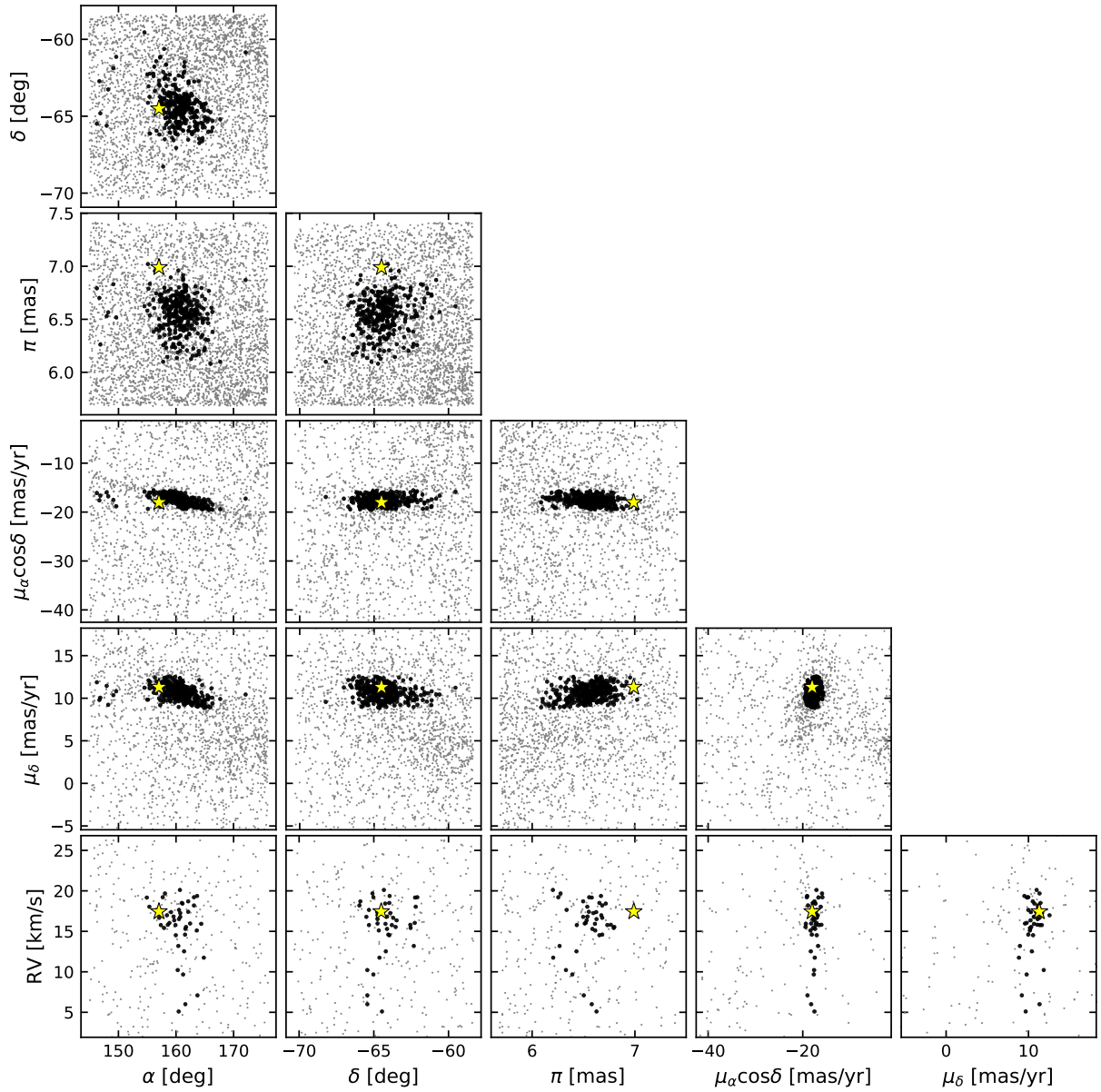

Figure 4. Positions and kinematics of TOI 837 (star), IC 2602 members (black circles), and stars in the neighborhood (gray circles). Members were identified by Cantat-Gaudin et al. (2018). α denotes right ascension, δ declination, π parallax, $\mu_{\rm delta}$ and μ_α proper motion in each equatorial direction, and RV radial velocity reported by Gaia-DR2. The RVs are for unblended spectra of bright stars ($G \lesssim 12$). The proper motion projection (μ_δ vs. $\mu_\alpha \cos\delta$) highlights the membership selection function.

The young open cluster members were selected for the presence of lithium, as described by Randich et al. (2018). The TOI-837 Li EW measured here (150 milliangstrom) is consistent with what's seen for stars of similar colors in <100 Myr old moving groups. (Elliott+2016, Fig 11 – attached). This is sensible, because IC 2602 is supposed to be 50 Myr old.

3.2.5. *Literature Membership*

The membership of TOI 837 in IC 2602 was noted by Oh et al. (2017), in what they dubbed "Group 5". Analyzing the clusters of Oh et al. (2017), **?** fitted the Gaia, 2MASS, and WISE photometry with MIST isochrones, and reported stellar masses, radii, metallicities, ages, distances, and extinction for 9754 stars, including TOI 837.

TOI 837 was also listed as a member of "Theia 92" by Kounkel & Covey (2019). These authors identified 999 candidate cluster members, and reported a cluster isochrone age $\log t = 7.55$ with uncertainty ≈ 0.15 dex. They reported an average extinction of Av=0.243 mag.

3.3. *Stellar Parameters*

3.3.1. *Physical*

(Lstar, Rstar, Teff, Age and Mstar)

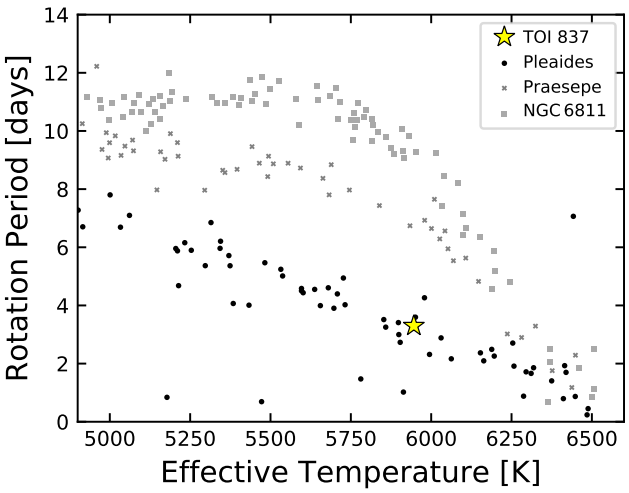

Figure 5. Rotation periods for TOI 837 and selected open clusters. The Pleiades (120 Myr), Praesepe (670 Myr), and NGC 6811 (1000 Myr) are shown. Their rotation periods were measured by Rebull et al. (2016); Douglas et al. (2017, 2019), and Curtis et al. (2019), respectively.

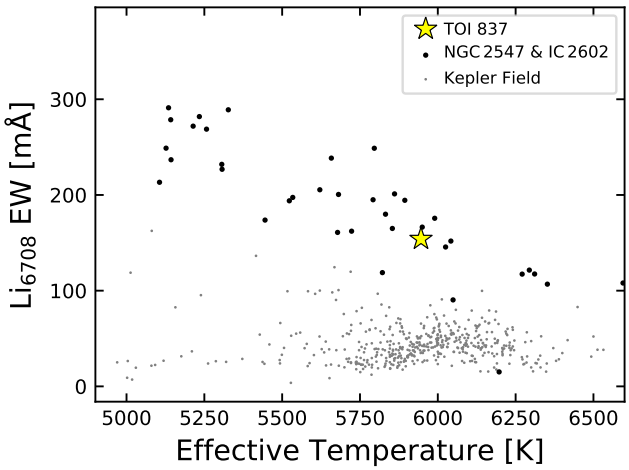

Figure 6. Lithium 6708Å equivalent widths for TOI 837, field stars, and young open clusters. The field star sample is drawn from Kepler planet hosts, and was measured by Berger et al. (2018) using Keck-HIRES. The young open clusters members were surveyed by Randich et al. (2018) using the UVES and GIRAFFE spectrographs at the ESO VLT. Randich et al. (2018) found lithium depletion boundary ages for these clusters of $37.7^{+5.7}_{-4.8}$ Myr (NGC 2547) and $43.7^{+4.3}_{-3.9}$ Myr (IC 2602).

From CHIRON spectra, my current best guess spectroscopic parameters are as follows. Teff = 5946 +/- 39 logg = 4.48 +/- 0.03 feh = -0.065 +/- 0.035 vsini = 17.48 +/- 0.15

Figure 7. The SED fit, looking really good with rchi2 = 1.6:

The fit parameters are: Av = 0.20 +/- 0.03 Fbol = 1.967 +/- 0.046 e-9 erg/s/cm2 Rstar = 1.049 +/- 0.019 Rsun

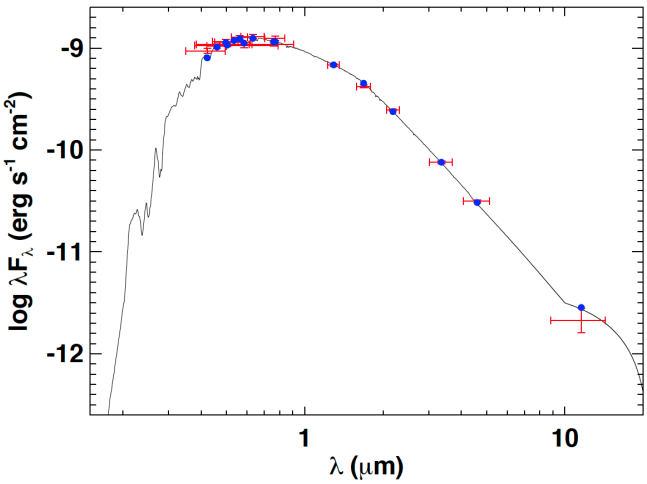

Figure 7. Spectral energy distribution of TOI 837 from archival photometry. Keivan: please describe, and if possible, send me the data (photometry + the atmosphere model) used to generate the plot so I can regenerate it in a consistent style with the rest of the paper

From the spectroscopic logg and the above Rstar, we get an independent mass estimate of Mstar = 1.21 +/- 0.10 Msun At face value, the mass seems a bit high for the radius, but I'm guessing that just means the spectroscopic logg is a bit too high.

Astrometric information—The RUWE (CITE, CITE) for TOI 837 is 1.02, indicative that there are no obviously present astometric companions.

3.3.2. *Rotation*

Stellar vsini Stellar rotation

3.4. *RVs*

I don't strongly expect the Veloce RVs or the FEROS ones to lead to a mass measurement. The reason is that with vsini=17km/s, and 2% rotation amplitude signal, we expect an RV RMS of 300m/s at the Prot=3.5 day rotation period (vsini*rotation amplitude). This is probably larger than the expected planet signal (100m/s, 8 days).

4. VALIDATION OF TOI 837.01

"""Validation is the process of statistically arguing that a transit-like signal is due to a planet rather than an astrophysical false positive. """ (CITE blender, Torres+04,05,10; vespa Morton 12, 15; pastis Diaz+14 Santerne+15; triceratops Giacalone & Dressing 20).

Many validation analyses are inherently flawed because they do not deal with the fact that you are conditioned on having observed many stars, and having found an eclipsing system.

Figure 8 provides a visual summary of the possible astrophysical false positive scenarios. If the TOI 837 signal is not planetary, it must come from the near-total eclipse of a background star (a BEB), or else a hierarchical companion of the

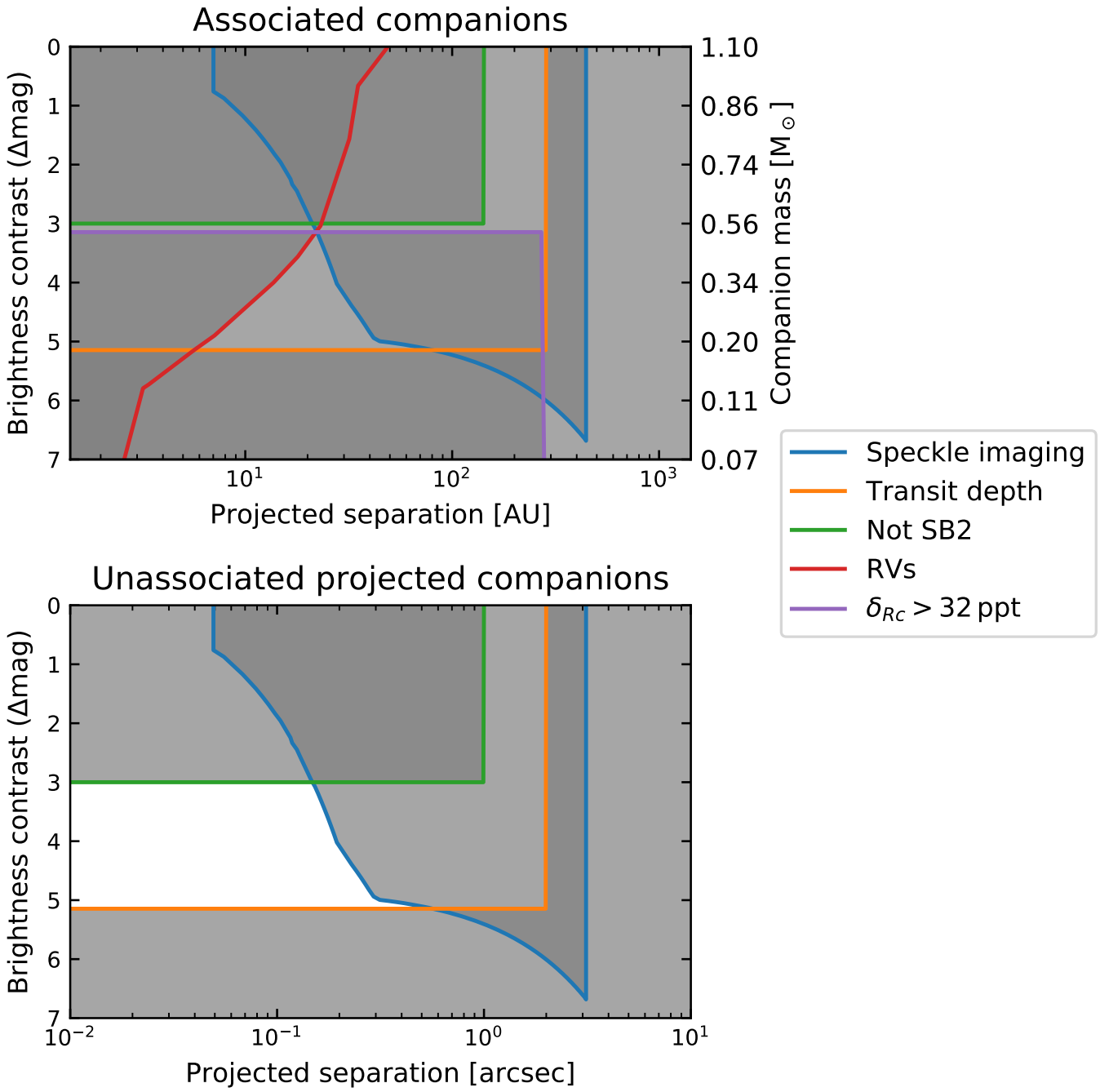

Figure 8. Astrophysical false positive scenarios. *Top*: for bound companions, *Bottom*: for unassociated companions along the same line of sight.

primary star (an HEB). It must also be verified that to the angular resolution possible, the transit signal originates from TOI 837, and not a neighboring star (an NEB). We proceed by describing each constraint in detail.

4.1. *Limits on Companions from the Transit Depth*

In HEB and BEB scenarios, the flux from TOI 837 and the true eclipsing binary host would blend together, reducing the "true" eclipse depth $\delta_{\rm true}$ to produce the observed depth $\delta_{\rm obs}$:

$$\delta_{\rm obs} = \delta_{\rm true} \frac{F_{\rm neighbor}}{F_{\rm total}}, \quad (1)$$

where the total flux and the flux from the neighbor are labelled as such. The requirement that the eclipse is produced by stars and that $\delta_{\rm true} < 0.5$ translates to a bound on the faintest possible blended companion stars:

$$\Delta m < -\frac{5}{2} \log_{10} \left(\frac{0.5}{\delta_{\rm obs}} \right). \quad (2)$$

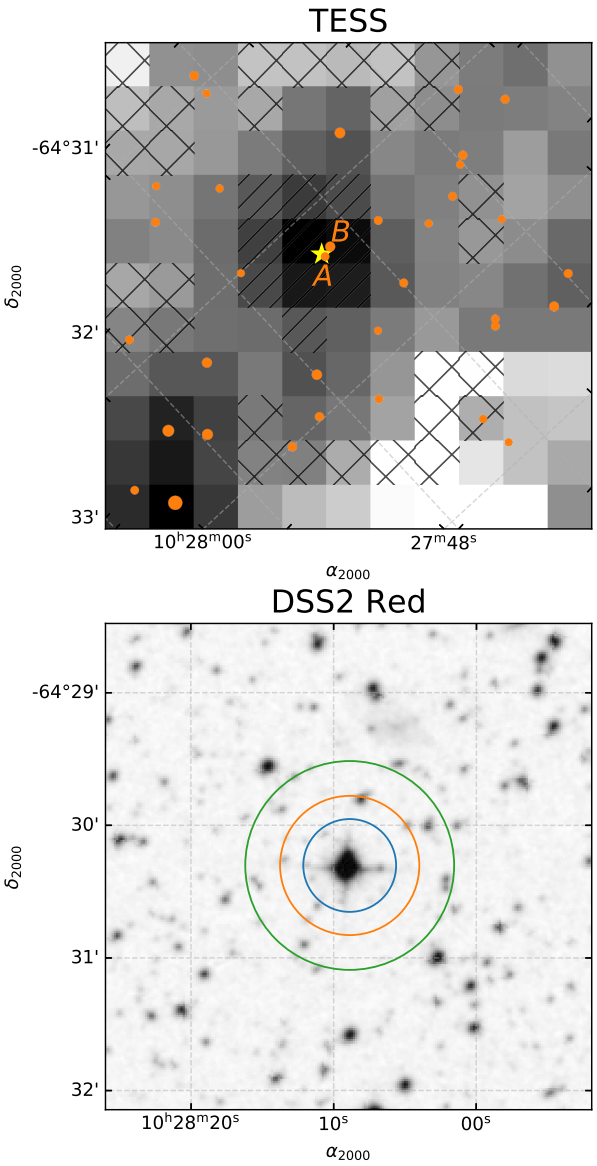

Figure 9. Scene used for blend analysis. *Top:* Mean TESS image of TOI 837 over Sector 10, with a logarithmic grayscale. The yellow star is the position of TOI 837. Orange circles are neighboring stars with $T < 16$, scaled such that brighter stars are larger. The X and / hatches show the apertures used to measure the background and target star flux, respectively. Dashed lines of constant declination and right ascension are shown. *Bottom:* Digitized Sky Survey *R*-band image of the same field, with a linear grayscale. The circles show apertures of radii 1, 1.5, and 2.25 pixels used in our blend analysis (Section 4). Two stars of interest are "Star A" and "Star B", which were eventually excluded as being possible sources of the transits.

For TOI 837 ($T = 9.93$), this implies that any stellar companion invoked to explain the transit depth must be brighter than $T = 15.07$.

Typically, the shape of the transits enables this argument to be scaled to even more restrictive depths (e.g., CITE

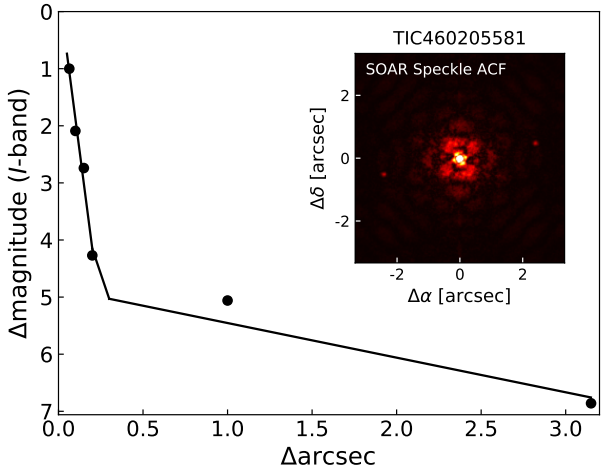

Figure 10. SOAR HRCam contrast limits derived from point-source injection-recovery experiments. Star A ($\Delta T = 4.7$, $\rho = 2.3$" west) is detected in the autocorrelation function, in addition to being a resolved Gaia source. It is co-moving with TOI 837, and its parallax and on-sky position imply that it is physically separated from TOI 837 by 6.6 ± 0.1 pc.

Seager 2003, Vanderburg+2019, Rizzuto+2020, David+2018 1298Tau). However, since the transits of TOI 837 are grazing, these arguments do not apply.

4.2. *Limits on Companions from Imaging*

4.2.1. *Gaia Imaging*

Figure 9 shows the scene as viewed in the DSS2 plates and by TESS. In the upper panels, the pixels used to measure the background level in the SPOC lightcurve are indicated with 'X' hatching, and the pixels used in the final lightcurve aperture are shown with '/' hatching.

Stars brighter than $T = 16$, as queried from the Gaia DR2 source catalog, are shown with orange circles. Given its galactic latitude of $b = -6°$, it is not surprising that the field of TOI 837 is crowded. The stars that were of immediate concern for a blend analysis were as follows.

- TOI 837 = TIC 460205581 (T=9.9). The target star.
- Star A = TIC 847769574 (T=14.6). 2.3" west. Proper motions and parallax imply it is comoving with TOI 837, though with a physical separation of 6.6 ± 0.1 pc, it may not be bound.
- Star B = TIC 460205587 (T=13.1). 5.4" north. This is a giant background star.

An additional source, TIC 847769581, is 4.9" from the target, but too faint (T=18.8) to be the source of the observed transit signal.

The Gaia DR2 data for Star A seems poorly behaved. While Star A has $G = 15.1$, and $Bp = 14.9$, no Rp magnitude is reported. Correspondingly, no RUWE value is available (CITE). The astrometric reduced χ^2 ($\chi^2/(N-5)$, for N the number of good astrometric observations) seems rather poor,

at 8.6. We suspect that the photometric failure to produce an *Rp* magnitude, as well as the poor astrometric fit, are likely due to blending with TOI 837.

At the angular resolution of the TESS data, if either Star A or Star B were eclipsing binaries, they could be the sources of the transit signal. We ruled out both Star A and Star B as hosts of the eclipse through a detailed analysis of the ground-based seeing-limited photometry (§ 2.2).

4.2.2. *Speckle Imaging*

Additional point-sources could be present beyond the angular resolution of the Gaia source catalog. To limit this possibility, we imaged the system using SOAR-HRCam, as described in Ziegler et al. (2020). **Carl: please describe**. The bandpass was a Johnson-Cousins, where I is centered at 879 nm and has a width of 289 nm.

Figure 10 shows the result. Star A (TIC 847769574) is detected as expected, and no additional companions are found. """ The points on the plot are measured 5-sigma detectable contrasts. The lines are linear smoothing fits between two regimes. In general, the sensitivity of speckle imaging to companions rises sharply from the diffraction limit to a "knee" at a separation of 0.15–0.2 arcseconds, where it then continues to slowly increase out to 1.5″, beyond which the speckle patterns become de-correlated. For this target, I suspect the measurement at 1″ is slightly larger than expected due to some increase in speckle noise at that radius. """

We convert the contrast ratios obtained through the SOAR imaging to constraints on the masses of putative companions following Montet+2014 (CITE and others!). We employed the Baraffe+2003 models for substellar mass objects and the MESA isochrones for stellar mass objects (Choi et al XXXX). We assumed that the system age was 35 Myr, to ensure that companions would be at a plausible state of contraction.

Due to the specific filters of the SOAR HRcam imager, we further assumed that all sources had blackbody spectra. While this is clearly false, we do not readily have access to the planetary and stellar atmosphere models needed for the correct calculation. However, the Baraffe+2003 and MESA models do report effective temperatures and bolometric luminosities. We opt to use these theoretical quantities, combined with the measured transmission functions, to calculate the absolute magnitudes in the HRCam bandpasses (CITE Tokovinin 2018 summary paper with the bandpasses).

4.2.3. *Archival Imaging*

Archival SERC-J and AAO-SES plates are available for the TOI 837 field[1]. These plates were acquired in 1982 and 1992, respectively. For high proper motion stars archival imagery can be used to detect slowly moving background stars that might be an astrophysical false-positive source (*e.g.*, Huang et al. 2018). However TOI 837 has only moved $\approx 0.7''$ between 1982 and present, in comparison to the $\approx 2.0''$ FWHM of the target on the plates. We therefore cannot resolve it with great confidence from background sources not already resolved through more modern imaging.

4.3. *Limits on Companions from Radial Velocities*

The combined radial velocities from FEROS, CHIRON, and Veloce can be used to place limits on the presence of massive, close-in bounds companion to TOI 837.

We derived the relevant limits using `radvel` (Fulton et al. 2018). We assumed circular orbits for the massive companion. We then fitted the RV data for the semiamplitude, period, time of conjunction, instrument offsets, and jitter parameters. We placed a wide log-uniform prior on the semiamplitude and period to ensure appropriate sampling of the relevant spaces. ($\log K \sim \mathcal{U}(1, 10^5)$, $\log P \sim \mathcal{U}(0.1, 10^{15})$).

We then converting the resulting posterior in period and semiamplitude to minimum mass and semi-major axis assuming Kepler's third law. The resulting 3σ limits are shown in Figure 8.

4.4. *Limits on Companions from Time-Series Photometry*

4.4.1. *TESS*

We examined the CDIPS FFI lightcurves of the target, which are available on MAST (Bouma et al. 2019). Three lightcurves are available, based on photometric apertures with a radius of 1, 1.5, or 2.5 pixels. In the raw difference-image light-curves, as well as the PCA-detrended light-curves, dips of depth ≈0.35% are visible, and their properties do not significantly vary with aperture size. Within ≈ 20", the dips are consistent with originating from the target star.

4.4.2. *Custom Apertures on Ground-Based Time-Series Photometry*

A total eclipse of Star A would produce a 1.4% dip. A 30% eclipse, more plausible for a NEB scenario, would produce dips of exactly the right depth (0.4%).

To assess this possibility with the ground-based photometry, we produced lightcurves centered on TOI 837 with circular apertures of radii ranging from 0.7″ to 5.1″. We did not detect any statistically significant variation in the depth of the transits.

We also created lightcurves with a custom set of $r = 2.1''$ apertures with positions ranging from Star A (2.3″ west of TOI 837) to 2.3″ east of TOI 837. We did not detect any variation of the transit depth along this line of lightcurves, as would be expected if Star A were the eclipse host. The apertures east of TOI 837 are particularly constraining, as they exclude over 90% of the flux from Star A. The eclipse on Star A would therefore need to be excessively deep to produce the observed eclipse depth. We take this to indicate that TOI 837 is the source of the transit signal to within ≈ 2.0″.

[1] https://archive.stsci.edu/cgi-bin/dss_form

4.4.3. *Color Photometry*

HEB and to a lesser extent BEB scenarios can be limited by color photometry. In the absense of color photometry, the most plausible HEB scenarios for TOI 837 involve pairs of eclipsing M dwarfs (Figure 8). These eclipses are redder than eclipses of the G-dwarf TOI 837. Observations that the transit depth does not decrease going to blue bands therefore limits the plausibility of these scenarios.

Simple Example—As a simple example, assume $M_2 = M_3 = 0.2M_\odot$ in a twin HEB. Assume PMS evolution, and use MIST isochrones for a 35 Myr system to convert between stellar properties. Take transmission functions (filters only; no instrument or atmosphere response) from the SVO filter profile service[2]. Integrate up blackbody functions over each bandpass for each star, and get estimates of the eclipse depths if there were a total eclipse (of either of the secondary or tertiary) with this set of parameters. The apparent eclipse depths in various Bessel and Cousins bandpasses are:

$$\begin{aligned}
\delta_{U_B} &= 5.03 \times 10^{-4} \text{ (Bessel U)} \\
\delta_{B_B} &= 1.39 \times 10^{-3} \text{ (Bessel B)} \\
\delta_{V_B} &= 3.31 \times 10^{-3} \text{ (Bessel V)} \\
\delta_{R_C} &= 5.59 \times 10^{-3} \text{ (Cousins R)} \\
\delta_{I_C} &= 9.69 \times 10^{-3} \text{ (Cousins I)} \\
\delta_{T} &= 9.18 \times 10^{-3} \text{ (TESS)} \qquad (3)
\end{aligned}$$

Our chief interest is the relative depths, because geometry lets all the depths be scaled to match the observed TESS depth of ≈43 ppt. (In this case, all depths would be scaled down by a multiplicative factor of 2.1).

The crucial point is that the bluest bands— U and B—are roughly 10 times shallower than TESS-band, because the M dwarf blackbody function turns over at 2 times longer wavelengths than the G dwarf blackbody (Wien's law).

Therefore if TOI 837 were a hierarchical eclipsing M dwarf pair, Phil's two R-band observations should have shown eclipses a factor of 1.64x shallower than TESS observed (so, 24ppt, instead of the 40ppt observed). So, the 40 (+/- 10ish) ppt R-band depths seen in Phil's transits vs TESS-band argue for a planet, but the level of confidence could probably be improved with U or B.

Limits on Masses of Bound Companions—With this intuition in place, we derived the limits on masses of bound hierarchical eclipsing companions as follows. We assumed that each system was composed of the primary (TOI 837), plus a tertiary companion eclipsing a secondary companion every 8.3 days.

For secondary masses ranging from 0.07 to 1.10 $M_\odot$, and mass ratios (M_3/M_2) from 0.1 to 1, we then calculated the observed maximal eclipse depth of Star 3 in front of Star 2 in a number of bandpasses. As before, we interpolated between mass, effective temperature, and radius assuming the MIST isochrones for a 35 Myr old system, and also assumed that each source had a blackbody spectrum.

We excluded systems for which the maximal eclipse depth in TESS-band was less than the observed depth (*i.e.*, systems for which the tertiary was too small). For the systems with maximal eclipse depths in TESS-band greater than the observed TESS-band depth, we then calculated the multiplicative factor required to shrink the depth (from the $b = 0$ case) to match the observed eclipse depth in the TESS-band. We then scaled the depths in each of the other bandpasses by this fixed geometric factor.

We then asked: given a fixed secondary mass, are there any tertiary companions for which the expected δ_{R_C} is larger than the observed Rc-band depth? In cases for which the answer was yes, we could not rule out such hierarchical eclipsing binary systems. Conversely, we were able to rule out systems for which at fixed secondary mass no tertiary mass would enable eclipses (in R_C-band) of the necessary depth.

For a lower limit on δ_{R_C} of 32 parts per thousand, we found that the transition between systems that would produce eclipses that no matter what were "too red", and systems that would produce eclipses that could be sufficiently blue happens in TOI 837 (for R_C-band) at $0.54M_\odot$. The corresponding limit is shown in Figure 8.

If we could obtain a similar limit in B-band, it would solidify this result (because it would drive the HEB system to be even bluer).

Limits on Masses of Projected Companions—Ignoring the effects of interstellar reddening, the constraint that $M_2 \gtrsim 0.54M_\odot$ based on colors applies to background eclipsing binaries as well. However, the blue eclipses produced by such systems (*e.g.*, a background G2V+K6V binary) can be kept while making the systems fainter by moving them to greater distances. The only way to definitively rule out such scenarios is to prove that the loss of light is from the target star, for instance by detecting the Rossiter-McLaughlin effect during a transit.

Such scenarios are somewhat contrived in that since no secondary eclipse is observed, they require either eccentric orbits to avoid secondary eclipses, or else a background twin binary system at double the orbital period.

[2] http://svo2.cab.inta-csic.es/theory/fps/

4.4.4. *Summary*

Possible false-positive scenarios are as follows.

- *Neighboring blends*. Ruled out to within 2 arcseconds by Phil Evans.
- *Hierarchical blends*. Limited by i) FEROS + Veloce RVs, and ii) speckle imaging. Multicolor photometry also limits.

  At present our data do not rule out the presence of bound companion stars from ≈10–100 AU, with masses in the range of ≈0.15–0.25 $M_\odot$ (Figure 8). Roughly 2-3% of Sun-like stars in the solar neighborhood with binary companions have companions in this region of parameter space (assuming the Raghavan+2010 CITE log-normal binary separation distribution, and a uniform companion mass function.)

  Companion statistics for hierarchical triples are somewhat less robust, but they have been studied, for instance by CITE Tokovinin 2014. CITE Tokovinin 2014 found that 7% of Sun-like stars are hierarchical triples with two companions in the compact orbit (the "L_{12}" configuration, rather than the "L_{11}" configuration of say, α Centauri). A priori then, given a Sun-like primary, the probability that it is in a hierarchical triple configuration in which the outer orbit satisfies the mass and semi-major axis constraints of Figure 8 is $\approx 7\% \times 3\% = 0.2\%$. This is independent of the issue that the inner pair would require finely tuned orbital parameters (i) to eclipse, and (ii) to be so compact.
- *Background blends*. An argument on the a priori probability of background blends follows from counting statistics. Within 360 arcseconds, there are 298 T<16 stars in TIC8 (i.e., Gaia DR2). At 2.0 arcseconds, SOAR archives dmag(I) of 6. Inside of 2 arcseconds, we expect πr^2 times (Nstar per sq arcsec) = 9e-3 T<16 stars. Any with T$\gtrsim$15 outside of 0.3 arcseconds would have been detected by SOAR, which brings down the expected number of possible hidden sources by a factor of a few. Within 0.3 arcseconds, where SOAR gets worse than dmag(I) of 3, we expect 2e-4 T<16 stars. So (order of magnitude), background blends would be a ∼0.1% coincidence.

5. THE PLANET

5.1. *Transit Fitting*

Simultaneous dip plus rotation period (GP) fit. Use celerite plus PyMC3/exoplanet. Mention FPP?

5.2. *Additional Transits*

None of the extra dips in the PDCSAP light-curve (e.g., "up-down" spikes at BTJD 1572 and 1601) seem likely to be planetary We checked that i) they were not present in the SAPFLUX light-curves, and ii) that they were not present in the CDIPS light-curves (either raw, or PCA-detrended).

To make this quantitative, we did injection-recovery.

6. DISCUSSION

In context,...

7. CONCLUSIONS

The authors thank... We also thank the Heising-Simons Foundation for their generous support of this work. The Digitized Sky Survey was produced at the Space Telescope Science Institute under U.S. Government grant NAG W-2166. Figure 9 is based on photographic data obtained using the Oschin Schmidt Telescope on Palomar Mountain. This research made use of the Exoplanet Follow-up Observation Program website, which is operated by the California Institute of Technology, under contract with the National Aeronautics and Space Administration under the Exoplanet Exploration Program. This research has made use of the SVO Filter Profile Service (http://svo2.cab.inta-csic.es/theory/fps/) supported from the Spanish MINECO through grant AYA2017-84089

Software: `astrobase` (Bhatti et al. 2018), `astropy` (Astropy Collaboration et al. 2018), `astroquery` (Ginsburg et al. 2018), `cdips-pipeline` (Bhatti et al. 2019) `corner` (Foreman-Mackey 2016), `exoplanet` (Agol et al. 2019) `exoplanet` (Foreman-Mackey et al. 2020), and its dependencies (Agol et al. 2019; Kipping 2013; Luger et al. 2019; Theano Development Team 2016). `IPython` (Pérez & Granger 2007), `lightkurve` (Lightkurve Collaboration et al. 2018), `matplotlib` (Hunter 2007), `MESA` (Paxton et al. 2011, 2013, 2015) `numpy` (Walt et al. 2011), `pandas` (McKinney 2010), `pyGAM` (Servén et al. 2018), `PyMC3` (Salvatier et al. 2016), `scipy` (Jones et al. 2001). `tesscut` (Brasseur et al. 2019), `webplotdigitzer` (Rohatgi 2019), `wotan` (Hippke et al. 2019).

Facilities: *Astrometry*: Gaia (Gaia Collaboration et al. 2016, 2018). *Imaging*: Second Generation Digitized Sky Survey, Keck:II (NIRC2; www2.keck.hawaii.edu/inst/nirc2). *Spectroscopy*: Keck:I (HIRES; Vogt et al. 1994). **VLT (number), UVES and GIRAFFE** (CITE: Pasquini et al 2002) *Photometry*: TESS (Ricker et al. 2015).

Table 1. Model Comparison.

Description	N_s	N_ℓ	N_{data}	N_{param}	χ^2	χ^2_{red}	BIC	ΔBIC
Favored	2	2	2585	17	3230.2	1.258	3363.7	0.0
Weakly favored	3	3	2585	21	3203.4	1.249	3368.4	4.7
—	3	2	2585	19	3222.9	1.256	3372.2	8.4
Disfavored	2	3	2585	19	3244.9	1.265	3394.2	30.4
—	2	1	2585	15	3410.6	1.327	3528.5	164.7
—	3	1	2585	17	3396.4	1.323	3530.0	166.3
—	1	2	2585	15	4158.6	1.618	4276.4	912.7
—	1	3	2585	17	4147.4	1.615	4281.0	917.2
—	1	1	2585	13	4313.5	1.677	4415.6	1051.9

NOTE— N_s and N_ℓ are the number of harmonics at the short and long periods, respectively. N_{data} is the number of fitted flux measurements. N_{param} is the number of free parameters in the model. The Bayesian information criterion (BIC) and the difference from the maximum ΔBIC are also listed.

Table 2. Best-fit model priors and posteriors.

Param.	Unit	Prior	Median	Mean	Std. Dev.	3%	97%
P_s	d	$\mathcal{N}(8.3247; 0.0050)$	8.3248321	8.3248295	0.0003356	8.3242288	8.3254817
$t_s^{(1)}$	d	$\mathcal{N}(1574.273800; 0.0050)$	1574.2727299	1574.2727323	0.0010770	1574.2707084	1574.2747189
$\log R_p/R_\star$	–	$\log\mathcal{U}(0.01; 1.00)$	-2.43072	-2.236	0.55106	-2.74890	-0.99823
b	–	$\mathcal{U}(0; 1+R_p/R_\star)$	0.9729	1.0221	0.1533	0.9165	1.2972
u_1	–	$\mathcal{U}(0.186; 0.486)^{(2)}$	0.335	0.335	0.088	0.187	0.469
u_2	–	$\mathcal{U}(0.075; 0.375)^{(2)}$	0.229	0.227	0.086	0.093	0.374
Mean	–	$\mathcal{U}(0.99; 1.01)$	1.000028	1.000028	0.000006	1.000016	1.000039
$R_\star$	$R_\odot$	$\mathcal{T}(1.05; 0.06)$	1.05	1.05	0.06	0.94	1.16
$\log g$	cgs	$\mathcal{N}(4.48; 0.09)$	4.46	4.46	0.08	4.32	4.61
$R_p/R_\star$	–	–	0.09	0.13	0.14	0.06	0.37
$\rho_\star$	g cm^{-3}	–	1.42	1.44	0.28	0.97	1.97
R_p	R_{Jup}	–	0.90	1.38	1.44	0.58	3.87
$a/R_\star$	–	–	17.33	17.35	1.11	15.28	19.33
$\cos i$	–	–	0.06	0.06	0.01	0.05	0.08
T_{14}	hr	–	1.79	1.79	0.05	1.68	1.87
T_{13}	hr	–	0.27	0.28	0.12	0.01	NaN

Note: T_{13} is ill-defined for a grazing transit.

(1) To convert mean TESS mid-transit time from BTJD to BJD_{TDB}, add 2,457,000.

(2) Assuming an informative quadratic limb-darkening prior with uniform values about those given for the appropriate T_{eff} and $\log g$ from Claret (2017).

REFERENCES

Agol, E., Luger, R., & Foreman-Mackey, D. 2019, arXiv e-prints, 1908.03222

Astropy Collaboration, Price-Whelan, A. M., Sipőcz, B. M., et al. 2018, AJ, 156, 123

Baratella, M., D'Orazi, V., Carraro, G., et al. 2020, Astronomy and Astrophysics, 634, A34

Berger, T. A., Howard, A. W., & Boesgaard, A. M. 2018, The Astrophysical Journal, 855, 115

Bhatti, W., Bouma, L., & Yee, S. 2019, `cdips-pipeline v0.1.0`, https://doi.org/10.5281/zenodo.3370324

Bhatti, W., Bouma, L. G., & Wallace, J. 2018, `astrobase`, https://doi.org/10.5281/zenodo.1469822

Bossini, D., Vallenari, A., Bragaglia, A., et al. 2019, Astronomy and Astrophysics, 623, A108

Bouma, L. G., Hartman, J. D., Bhatti, W., Winn, J. N., & Bakos, G. Á. 2019, ApJS, 245, 13

Brasseur, C. E., Phillip, C., Fleming, S. W., Mullally, S. E., & White, R. L. 2019, Astrophysics Source Code Library, ascl:1905.007

Bravi, L., Zari, E., Sacco, G. G., et al. 2018, Astronomy and Astrophysics, 615, A37

Cantat-Gaudin, T., Jordi, C., Vallenari, A., et al. 2018, Astronomy & Astrophysics, 618, A93

Claret, A. 2017, Astronomy & Astrophysics, 600, A30, arXiv: 1804.10295

Curtis, J. L., Agüeros, M. A., Douglas, S. T., & Meibom, S. 2019, The Astrophysical Journal, 879, 49

Douglas, S. T., Agüeros, M. A., Covey, K. R., & Kraus, A. 2017, The Astrophysical Journal, 842, 83

Douglas, S. T., Curtis, J. L., Agüeros, M. A., et al. 2019, The Astrophysical Journal, 879, 100

Foreman-Mackey, D. 2016, The Journal of Open Source Software, 24

Foreman-Mackey, D., Czekala, I., Luger, R., et al. 2020, exoplanet-dev/exoplanet v0.2.6

Fulton, B. J., Petigura, E. A., Blunt, S., & Sinukoff, E. 2018, PASP, 130, 044504

Gaia Collaboration, Prusti, T., de Bruijne, J. H. J., et al. 2016, A&A, 595, A1

Gaia Collaboration, Brown, A. G. A., Vallenari, A., et al. 2018, A&A, 616, A1

Ginsburg, A., Sipocz, B., Madhura Parikh, et al. 2018, Astropy/Astroquery: V0.3.7 Release

Hippke, M., David, T. J., Mulders, G. D., & Heller, R. 2019, arXiv:1906.00966 [astro-ph], arXiv: 1906.00966

Huang, C. X., Burt, J., Vanderburg, A., et al. 2018, ApJ, 868, L39

Hunter, J. D. 2007, Computing in Science & Engineering, 9, 90

Jenkins, J. M., Twicken, J. D., McCauliff, S., et al. 2016, Software and Cyberinfrastructure for Astronomy IV, 9913, 99133E

Jones, E., Oliphant, T., Peterson, P., et al. 2001, Open source scientific tools for Python

Kharchenko, N. V., Piskunov, A. E., Schilbach, E., Röser, S., & Scholz, R.-D. 2013, Astronomy and Astrophysics, 558, A53

Kipping, D. M. 2013, MNRAS, 435, 2152

Kounkel, M., & Covey, K. 2019, The Astronomical Journal, 158, 122

Lightkurve Collaboration, Cardoso, J. V. d. M., Hedges, C., et al. 2018, Lightkurve: Kepler and TESS time series analysis in Python, Astrophysics Source Code Library, ascl:1812.013

Luger, R., Agol, E., Foreman-Mackey, D., et al. 2019, AJ, 157, 64

McKinney, W. 2010, in Proceedings of the 9th Python in Science Conference, ed. S. van der Walt & J. Millman, 51

Netopil, M., Paunzen, E., Heiter, U., & Soubiran, C. 2016, Astronomy and Astrophysics, 585, A150

Oh, S., Price-Whelan, A. M., Hogg, D. W., Morton, T. D., & Spergel, D. N. 2017, The Astronomical Journal, 153, 257

Paxton, B., Bildsten, L., Dotter, A., et al. 2011, ApJS, 192, 3

Paxton, B., Cantiello, M., Arras, P., et al. 2013, ApJS, 208, 4

Paxton, B., Marchant, P., Schwab, J., et al. 2015, ApJS, 220, 15

Pérez, F., & Granger, B. E. 2007, Computing in Science and Engineering, 9, 21

Randich, S., Tognelli, E., Jackson, R., et al. 2018, Astronomy & Astrophysics, 612, A99

Rebull, L. M., Stauffer, J. R., Bouvier, J., et al. 2016, The Astronomical Journal, 152, 113

Ricker, G. R., Winn, J. N., Vanderspek, R., et al. 2015, Journal of Astronomical Telescopes, Instruments, and Systems, 1, 014003

Rohatgi, A. 2019, WebPlotDigitizer: v4.2

Salvatier, J., Wieckiâ, T. V., & Fonnesbeck, C. 2016, PyMC3: Python probabilistic programming framework

Servén, D., Brummitt, C., & Abedi, H. 2018, dswah/pyGAM: v0.8.0

Stassun, K. G., Oelkers, R. J., Pepper, J., et al. 2018, AJ, 156, 102

Stassun, K. G., Oelkers, R. J., Paegert, M., et al. 2019, arXiv:1905.10694 [astro-ph], arXiv: 1905.10694

Theano Development Team. 2016, arXiv e-prints, abs/1605.02688

Vogt, S. S., Allen, S. L., Bigelow, B. C., et al. 1994, SPIE Conference Series, ed. D. L. Crawford & E. R. Craine, Vol. 2198

Walt, S. v. d., Colbert, S. C., & Varoquaux, G. 2011, Computing in Science & Engineering, 13, 22

Ziegler, C., Tokovinin, A., Briceño, C., et al. 2020, AJ, 159, 19